Correlations between Growth Kinetics and Microstructure for Scales Formed by High-Temperature Oxidation of Pure Nickel. II. Growth Kinetics

R. Peraldi,* D. Monceau,*† and B. Pieraggi*

The oxidation kinetics of high-purity nickel were studied between 500 and 1200°C, in pure oxygen at atmospheric pressure, for average oxide-scale thicknesses of 1, 5, 10, and 30 μm. In the overall temperature range studied, a decrease in the parabolic rate constant k_p with increasing scale thickness was observed. Depending on temperature and oxide-scale thickness, growth kinetics can be interpreted as a mixture of parabolic- and cubic-growth kinetics. Possible correlations between growth kinetics and microstructures of the oxide scales were investigated. From this set of experimental data, oxidation-kinetics models were tested. In particular, the effect of grain-boundary diffusion on NiO-growth kinetics was discussed. The correlations between growth kinetics and oxide microstructures appear to be more complex than usually reported.

KEY WORDS: Ni oxidation; growth kinetics; k_p; grain-boundary diffusion.

INTRODUCTION

In the preceding paper (Part I), NiO-surface morphologies and internal microstructures were characterized over a wide range of temperature (450–1200°C) and for scale thickness ranging from 1 to 70 μm. The present paper presents experimental data permitting an accurate analysis of the growth kinetics of the previously observed NiO scales. Possible correlations between

*CIRIMAT UMR 5085 (INPT/UPS/CNRS), ENSIACET, 118 Route de Narbonne, F-31077 Toulouse, Cedex 04, France.
†To whom all correspondence should be sent; email: daniel.monceau@ensiacet.fr

scale-growth kinetics, morphologies, and microstructures of NiO scales were investigated in order to reach a better understanding of the growth mechanisms. Indeed, despite the apparent simplicity of the system studied, numerous parameters, such as, metal purity, surface preparation, substrate orientation, and test procedure are known to affect the growth kinetics of NiO scales.

LITERATURE REVIEW OF Ni-OXIDATION KINETICS

Values of parabolic rate constants k_p for the growth of NiO found in the literature correspond to various experimental conditions (sample purity, crystallographic orientation, surface preparation, oxygen partial pressure, and temperature) as summarized in Table I. These values of k_p are presented in a common Arrhenius plot (Fig. 1) to be compared at: high temperatures (>1000°C), intermediate temperatures (1000–600°C) and low temperatures (<600°C).

Values of parabolic rate constants are in good agreement for temperatures higher than 1000°C (Fig. 1). In this temperature range, the activation energy for k_p, and the activation energy for nickel volume diffusion through NiO scales, range, respectively, from 180 to 240 kJ/mol^{-1} (Table I), and from 154 to 254 kJ/mol^{-1}.[1–6] Comparison of these values leads to the assumption that the outward diffusion of cationic species is the main mechanism controlling the NiO scale-growth kinetics at these temperatures.[7–10].

At intermediate temperatures, parabolic rate constants are more widely distributed (Fig. 1). Several explanations have been proposed in the literature: sample purity could explain variations between growth rates as impurities could affect the vacancy concentration in NiO.[9] The sample surface preparation (mechanically, chemically or electrochemically polished, annealed) could dramatically modify the scale-growth kinetics.[11–15] Furthermore, the crystallographic orientation of nickel grains plays an important role: oxidation of the oriented (100) nickel face is more rapid than oxidation of (110), (111), and (112) oriented faces.[16–20] Whatever the differences observed between growth kinetics at intermediate temperatures, the overall shape of the Arrhenius plot (Fig. 1) shows a transition in a temperature range of approximately 900–1000°C.[9,21] For intermediate temperatures, the activation energy (Table I) ranges from 80 to 100 $kJ\,mol^{-1}$ showing that growth mechanisms are different than for the highest temperatures (Fig. 2). The parabolic rate constants k_p obtained at intermediate temperatures indicate that oxide-scale growth is more rapid at these temperatures than predicted from nickel bulk-diffusion data.[22] It was generally accepted that short-circuit diffusion of nickel through NiO could significantly increase the scale-growth kinetics and grain-boundary diffusion was often evoked.[23]

Table I. Experimental Conditions for the Determination of k_p Found in the Literature Concerning the Oxidation of Pure Nickel

Ref.	Year	Purity	T (°C)	P_{O_2}[a] (atm)	Mono. or poly[b]	Surface preparation[c]	Ea (kJ · mol^{-1})
8	1952	99.9	400–900	0.1	Poly.	A + PO at 300 or 500°C	145
12	1954	99.98	400–750	0.1	Poly.	MP or EP + A	172
7	1965	99.90	900–1400	Diss. to 1	Poly.	MP + A	182
35	1968	99.94	500–600	1	Poly.	MP	158
9	1968	99.95	600–1400	1	Poly.	MP + CP + A	204 and 100
9	1968	99.975	600–1400	1	Poly.	MP + CP + A	238 and 100
9	1968	99.985	700–1100	1	Poly.	MP + CP + A	238 and 100
17	1972	99.999	500–800	0.5	Mono. (100), (110), (111)	A + EP	84, 54, 117
40	1972	99.998	700–1270	1	Poly.	CP + EP + A + CP + EP	
40	1972	99.998	700–1270	1	Poly.	CP + EP + A + MP	
38	1972	99.998	23–450	6.6×10^{-6} to 7.9×10^{-4}	Poly.	MP + EP	171
41	1985	99.995	800–1227	0.01 to 1	Poly.	MP + PO at 1200°C	225
14	1993	99.99	600–800	6.6×10^{-6}	Poly.	MP + A + MP	88 ± 17
14	1993	99.99	600–800	6.6×10^{-6}	Poly.	MP + A + CP	100 ± 25
15	1995	99.99	700–800	6.6×10^{-6}	Mono. (100) (111) Poly.	MP + A + MP or CP	
42	1995	99.995	600–1200	1	Poly.	MP + A	

[a] "Dis." corresponded to the dissociative oxygen partial pressure of NiO.

[b] "Mono" and "Poly", respectively, corresponded to monocrystalline or polycrystalline samples.

c "A," "PO," "MP," "CP," and "EP," respectively, corresponded to sample preparation: anealing, pre-oxidizing, mechanically or chemical or electrochemical polish.

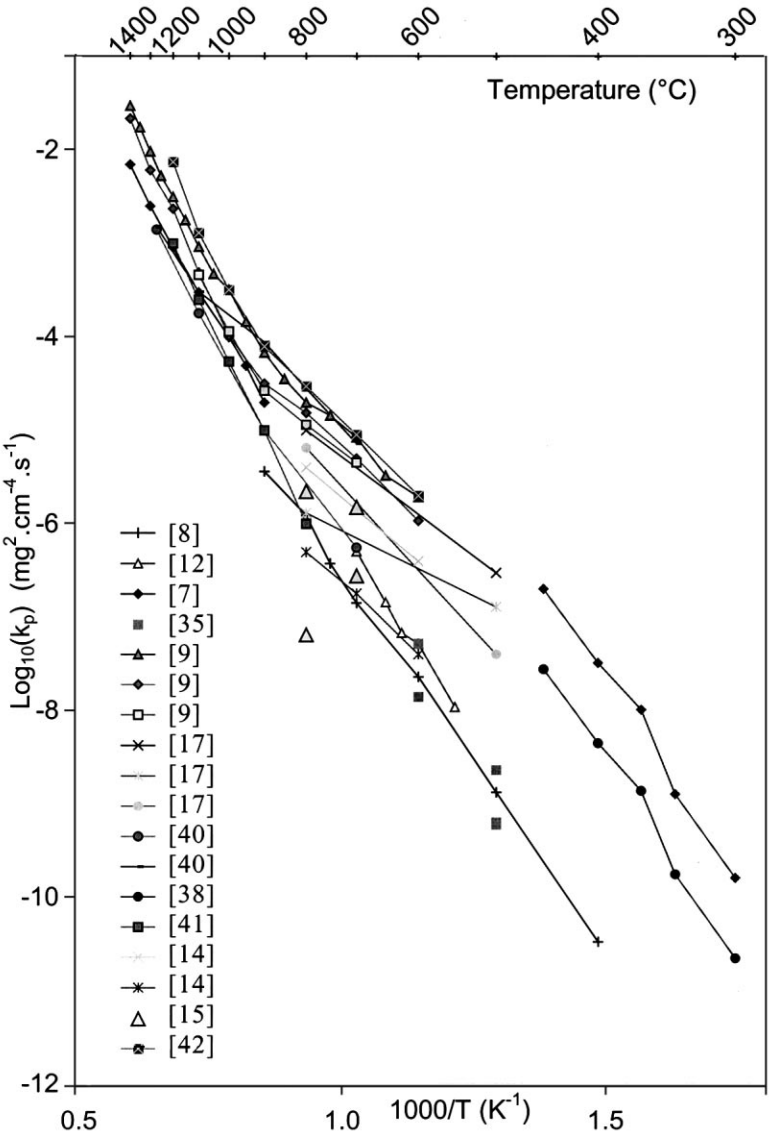

Fig. 1. Literature review of parabolic rate constants k_p for the isothermal oxidation of nickel.

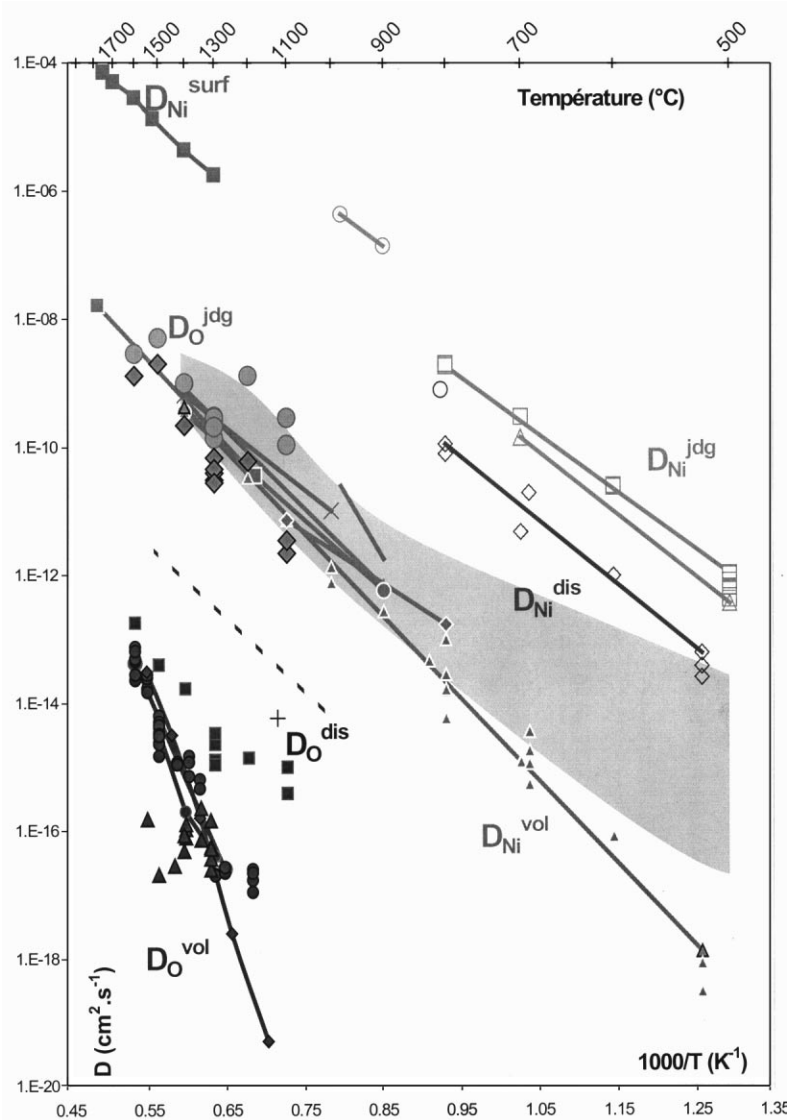

Fig. 2. Bibliographic survey of nickel, and oxygen-diffusion data in NiO (volume, grain-boundary, dislocation, and surface diffusion).[1–7,25,26,33,43–49] The values of parabolic constants reported in Fig. 1 are superposed using Wagner's relationship between D and k_p.

However, grain-boundary, nickel-diffusion measurements were all determined from NiO polycrystals formed by the total oxidation at 1100°C,[24] 1200°C,[25] or 1400°C[26] of thin-nickel foils. Possible artifacts linked to this method were revealed by Barbier *et al.*[27] and experiments on bicrystals or sintered polycrystals failed to reveal any enhancement of diffusion along the grain boundaries[28–30], within a detection limit of about $D_{GB}/D_{VOL} \sim 10^3$. Atkinson *et al.*[30] attributed this last effect to grain-boundary segregation, in disagreement with other measurements on similar samples.[27]More recently, molecular-dynamics (MD) calculations[31] of volume and grain-boundary diffusion of nickel gave an enhancement factor of about 10^3, i.e., far below the $10^{5.5}$ to $10^{6.5}$ factor found between 500 and 800°C in oxidized foils.[24, 25] MD calculations were also recently performed for the surface diffusion of nickel vacancies,[32] but only at very high temperatures (>1400°C). Measurements of surface diffusion between 1300 and 1750°C were previously performed from the analysis of grain-boundary grooving.[33] These latter values were close to the high-temperature extrapolation of grain-boundary diffusion coefficients determined for oxidized nickel foils. Finally, doubt exists concerning the nature of the fast diffusion paths in nickel oxide scales.[34]

At intermediate temperatures, a decrease in the parabolic rate constant with oxidation time was observed.[12,17,23,35] Grain-boundary diffusion could explain this evolution as oxide grain size increases with time. Rhines *et al.*[36,37] observed a proportional relationship between the volume of NiO grains and time so that a proportional relationship between weight-gain and cubic root of time is satisfied. Indeed a cubic-kinetics law could be observed between 800 and 1000°C.

There are only few data available on oxidation at temperatures lower than 600°C (Fig. 1). Dispersion between the reported values is large and could be explained by the influence of sample purity and surface preparation. Logarithmic-growth kinetics for thinner scales and parabolic growth kinetics for thicker scales were proposed.[38]

EXPERIMENTAL PROCEDURE

Thermogravimetric Analysis

Heat treatments (annealing and oxidation) were performed in a SETARAM TAG 24S thermobalance. The principle of such a thermobalance is the use of a symmetrical double furnace designed to compensate signal perturbations resulting from gas flow, buoyancy, and convection. Therefore, mass-change measurements were not sensitive to changes in gas flow and temperature and could be recorded very accurately during long-term exposures, and during heating or cooling periods, or else during gas

switching. The accuracy of this thermobalance is better than 1 μg at all temperatures. Furnace temperatures are controlled using Pt/Pt–Rh 10% thermocouples with an accuracy of better than ±1°C.

The oxidation tests were performed between 500 and 1200°C under a fixed oxygen flow of $0.2\,l \cdot h^{-1}$. To compare and analyze the oxide scale-growth kinetics within this temperature range, oxidation tests were interrupted at weight gains corresponding to average scale thicknesses of 1, 5, 10, 30, and 70 μm, thus leading to oxidation durations ranging from 10 min to 1 month.

Determination of Parabolic Rate Constant k_p

Scale-growth kinetics were interpreted by using the most-general expression for parabolic kinetics:[39]

$$t = a + b\Delta m + c\Delta m^2 \tag{1}$$

where Δm is the weight gain per unit area ($mg\,cm^{-2}$) and t the time (s). In Eq. (1), the coefficient c is equal to the reciprocal of the parabolic rate constant k_p ($mg^2 \cdot cm^{-4} \cdot s^{-1}$), independent of the initial condition for integration of the rate equation.[39] Equation (1) could be fitted to the entire set of $(t, \Delta m)$ data to get a global value of k_p. Moreover, Eq. (1) could also be fitted only to a smaller part of $(t, \Delta m)$ data to determine the local and instantaneous k_p values, representative of given time or scale thickness intervals. Therefore, variations of k_p as a function of time or scale thickness could be studied. For this last calculation, the size of the mass-gain interval fit was increased proportionally to the time squared in order to keep a constant noise/signal ratio.

Comparison of Constant, Linear, Parabolic, and Cubic Terms of Growth Rate

As large variations of k_p as a function of scale thickness are often observed, other fitting equations were also tested. The cubic form:

$$t = a + b\Delta m + c\Delta m^2 + d\Delta m^3 \tag{2}$$

was also used to fit the mass-gain curves at 700, 800, 900, and 1100°C. A comparison of the weights of the constant, linear, parabolic, and cubic terms of the growth rate given by Eq. 2 was obtained by calculating, respectively, the A, B, C, and D terms:

$$A = \frac{a}{t} \tag{3}$$

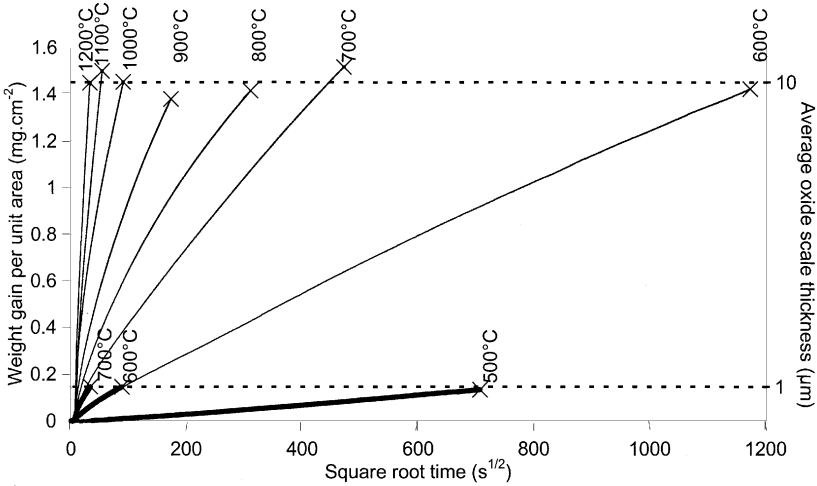

Fig. 3. Weight-gain curves vs. square root of time during oxidation of pure nickel for average NiO scales thicknesses of approximately 1 μm obtained in the temperature range 500–700°C and for average scales thicknesses of NiO of approximately 10 μm obtained in the temperature range 600–1200°C.

$$B = \frac{b(\Delta m)}{t} \tag{4}$$

$$C = \frac{c(\Delta m)^2}{t} \tag{5}$$

$$D = \frac{d(\Delta m)^3}{t} \tag{6}$$

with

$$A + B + C + D = 1 \tag{7}$$

RESULTS

Weight-Gain Curves

Weight-gain curves during isothermal oxidation of pure nickel are shown versus square root of time (Fig. 3). Oxidation runs between 450 and 1200°C were interrupted for average scales thicknesses of approximately 1, 5, 10, and 30 μm. For the sake of clarity, only weight-gain curves corresponding to average oxide-scale thicknesses of approximately 1 μm (obtained in the temperature range 500–700°C) and of approximately 10 μm

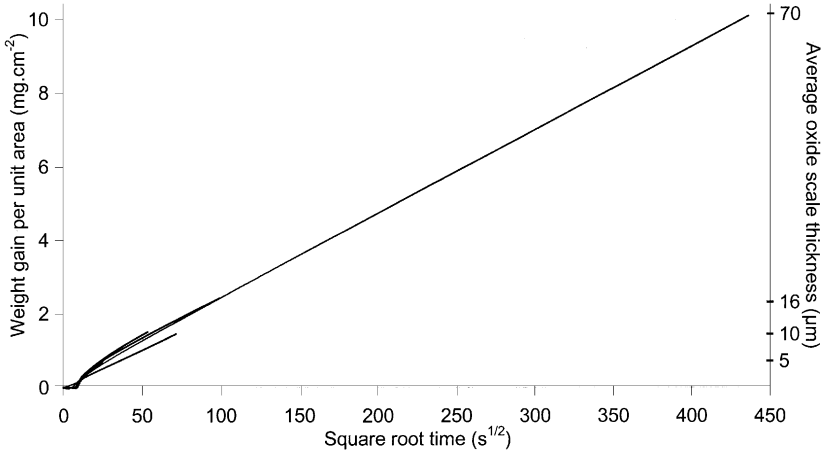

Fig. 4. Weight-gain curves vs. square-root of time during oxidation of pure nickel for average NiO scales thicknesses of approximately 5, 10, 16, and 70 μm obtained at 1100°C.

(obtained in the temperature range 600–1200°C) are shown in Fig. 3. As oxidation experiments were compared for a same average NiO scale thickness and were obtained in a large temperature range, test durations were very different: 389 hr at 600°C and only 20 min at 1200°C for an oxide-scale thickness of 10 μm. The (Δm, $t^{1/2}$) weight-gain curves were not linear (particularly for lower temperature), showing a deviation from the simple parabolic law ($\Delta m^2 = k_p t$). Indeed, at 1100°C, weight-gain curves versus square-root of time for an average oxide scale thickness ranging from 5 to 70 μm were linear only for scales thicker than 5 μm (Fig. 4). At 700°C, weight-gain curves were not linear whatever the scale thickness, ranging from 1 to 30 μm (Fig. 5). For all tested temperatures, weight gains during the first minute of the oxidation test should not be taken into account. This corresponded to the necessary time for oxygen to reach the sample after evacuation and gas switching from argon. The comparison of weight-gain curves obtained for a same temperature (Figs. 4 and 5) showed good reproducibility of the experiments.

Effect of Temperature on the Global Parabolic Rate Constants k_p

The reproducibility of weight-gain curves permitted an accurate determination of the global parabolic rate constants k_p calculated from Eq. 1. These global k_p values, as a function of scale thickness and temperature, are reported in Fig. 6. The general shape of $\log(k_p)$ variation as a function of the reciprocal temperature was found to be more complex than usually

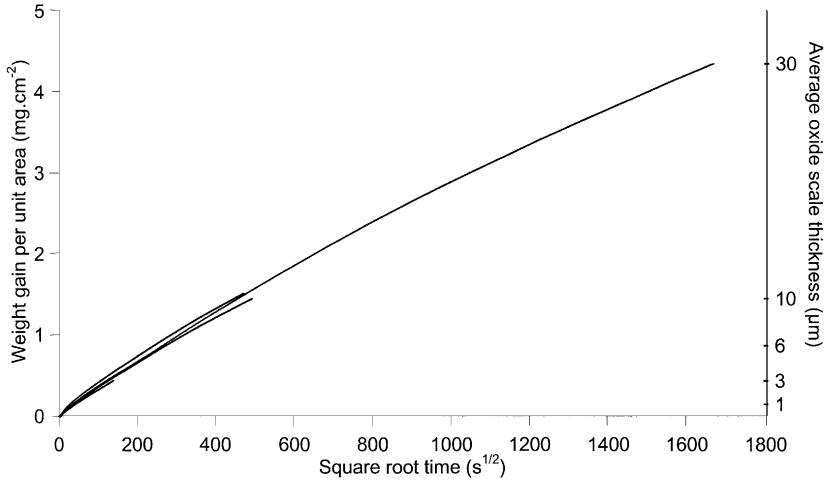

Fig. 5. Weight-gain curves vs. square-root of time during oxidation of pure nickel for average NiO scales thicknesses of approximately 1, 3, 6, 10, and 30 μm obtained at 700°C.

reported in the literature. Indeed, two changes of slope were observed: the first one at approximately 900°C and the second one at approximately 700°C. For all temperatures studied, parabolic rate constants decreased with increasing oxide-scale thickness. Between 1000 and 1200°C, the decrease in k_p was large for scale thickness between 1 and 5 μm then lower values of parabolic rate constants were stabilized for thicker scales. At temperatures lower than 1000°C, no stabilization of parabolic rate constants was observed, even for scale thickness of 30 μm. At 600°C, the decrease in k_p appeared less significant. However, scales thicker than 10 μm could not be obtained at this temperature as a 10-μm thick scale already required 380 hr of oxidation.

Large variations in parabolic rate constants with increasing oxide-scale thickness lead to difficulty in the calculation of the activation energy. Nevertheless, for high temperatures (>1000°C) and thick NiO scales (>10 μm), parabolic rate constants were stabilized and allowed a determination of an activation energy equal to 200 ± 5 kJ/mol^{-1}. This value is in good agreement with those calculated in previous works (180 and 240 kJ/mol^{-1}).

Decrease of Instantaneous k_p with Increasing Oxide-Scale Thickness

For tests performed at 700, 800, 900, and 1100°C, variations in k_p as a function of scale thickness, were better characterized by the calculated

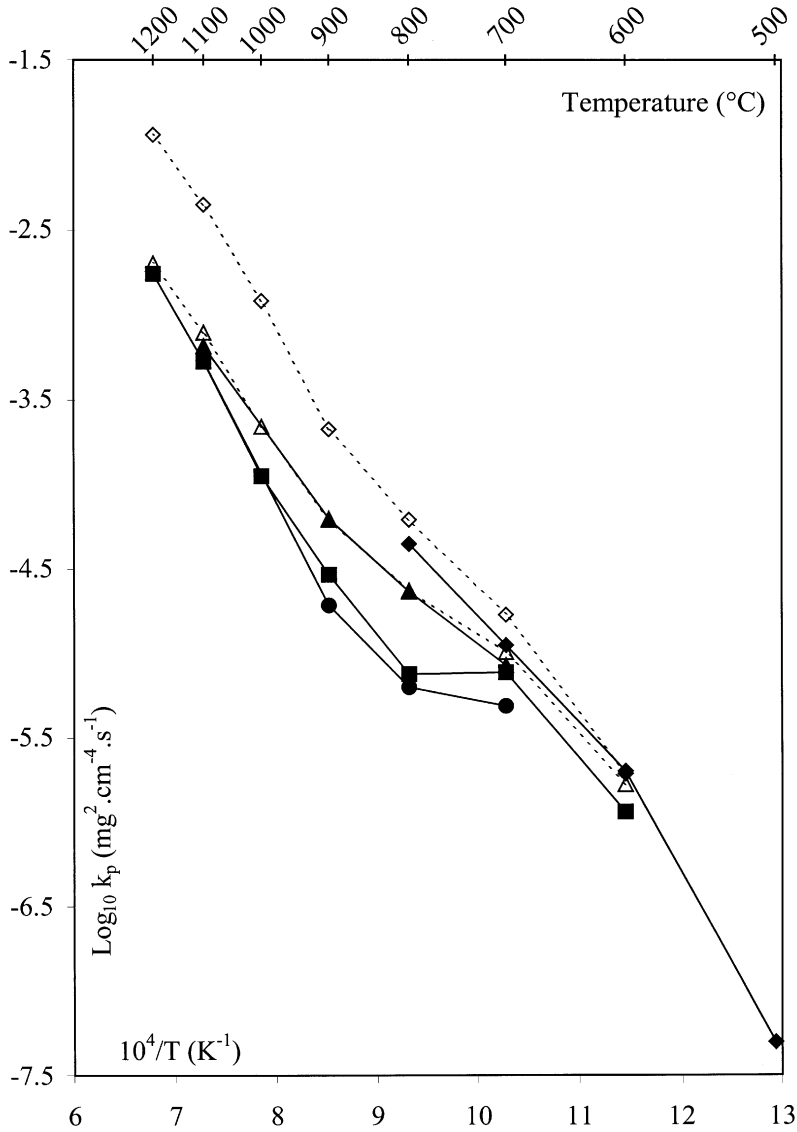

Fig. 6. Arrhenius plot of global parabolic rate constants k_p as a function of test temperature and scale thicknesses of approximately 1 (◆), 5 (▲), 10 (■), and 30 μm (●). White symbols indicated values of k_p calculated for scales thicknesses of 1 (◇) and 5 μm (△) from weight-gain curves of experiments corresponding to oxide-scale thickness of approximately 10 μm.

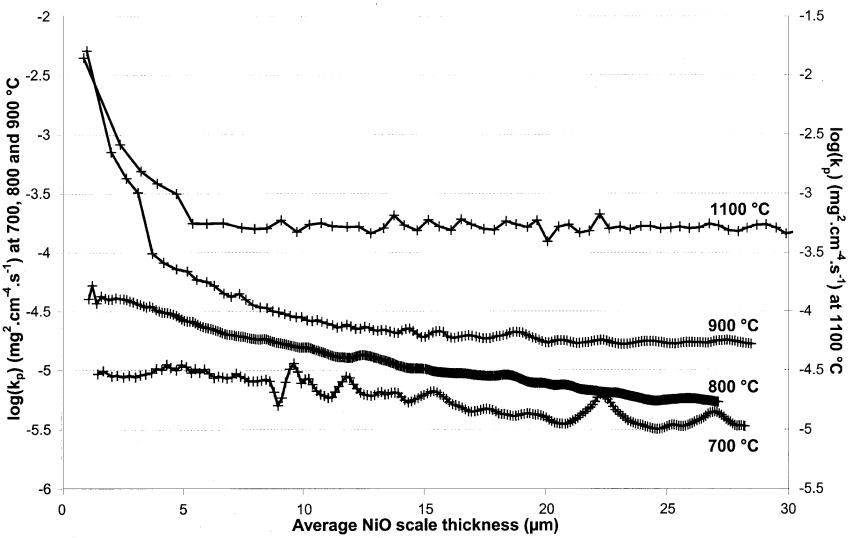

Fig. 7. Variations of the instantaneous parabolic rate constants k_p with increasing average oxide-scale thickness for NiO layers grown at 700, 800, 900, and 1100°C.

instantaneous k_p values (Fig. 7). These calculations were made for the thickest scales of approximately 30 μm. The behavior of global k_p in an Arrhenius plot (Fig. 6) was confirmed with instantaneous k_p variations. At 1100°C, for a scale thickness ranging from 1 to 5 μm, an initial fast and large decrease (by a factor of 30) was observed (Fig. 7). No significant variation in k_p was noticed for thicker scales. At this stage, the scale-growth kinetics could be accurately described by the usual form of parabolic kinetics. At 800 and 700°C, instantaneous k_p continuously decreased as the scale thickness increased between 1 and 30 μm (Fig. 7). However, the amplitude of this decrease (factors of 10 and 3, respectively) was smaller than at 1100°C. The temperature of 900°C corresponded to an intermediate behavior, where k_p was stabilized for scales thicker than 20 μm. However, at 900°C, for a scale thickness ranging from 1 to 20 μm, the amplitude of the decrease in k_p was the largest (factor 300). Such a behavior implied that the scale-growth kinetics could not be described by the usual form of parabolic kinetics given by Eq. (1).

Cubic Kinetics

As the scale-growth rate decreased faster than predicted by the normal parabolic kinetics, some attempts to analyze the scale-growth kinetics using

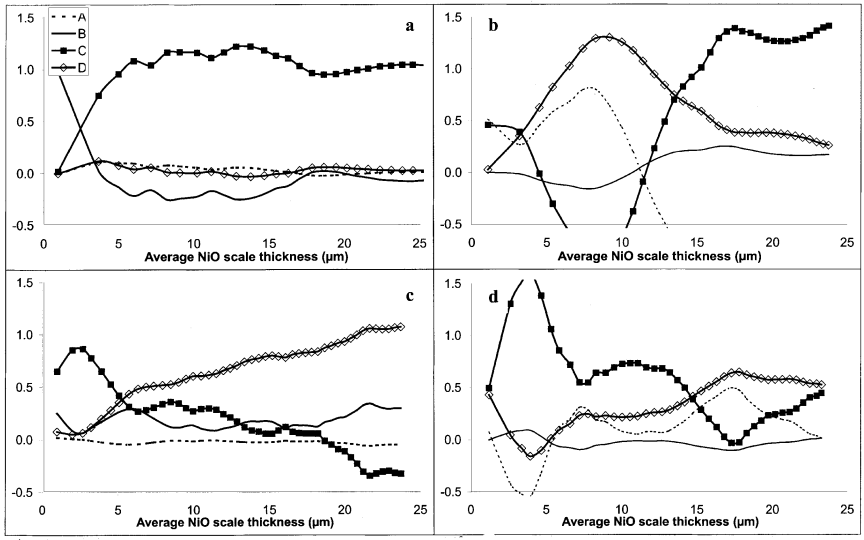

Fig. 8. Variations of scale-growth kinetics terms $A = a/t$, $B = b\Delta m/t$, $C = c\Delta m^2/\mathrm{t}$ and $D = d\Delta m^3/t$, as a function of average NiO-scale thicknesses: (a) 1100°C; (b) 900°C; (c) 800°C, and (d) 700°C.

a cubic law were made. Such cubic kinetics were already reported by Rhines *et al.*[36] for NiO scales grown between 800 and 1000°C. Therefore, weight-gain data were also fitted assuming cubic kinetics of the form of Eq. (2) (Fig. 8). This procedure is used to detect time intervals where terms A, B, C, and D are constant and to compare the relative weights of the linear, parabolic, and cubic terms in these intervals. Transient regimes may lead to negative values of terms A, B, C, and D, and should be disregarded here. For tests performed at 1100°C (Fig. 8a), the observed variations of terms A, B, C, and D show quite clearly that the scale-growth kinetics were parabolic for NiO scales thicker than 5 μm. This result is in good agreement with the decrease of instantaneous parabolic rate constants (Fig. 7). Between 1 and 5 μm, the largest term was the linear term showing that either interfacial reactions or some transient stage mostly controlled the growth kinetics. At 900°C, the growth kinetics were cubic and then parabolic for oxide scales thicker than 15 μm. This pure-parabolic behavior was in good agreement with the constancy of instantaneous k_p (Fig. 7). At 800 and 700°C, the parabolic term C was the most important for scale thicknesses ranging from 1 to 5 μm and from 1 to 15 μm, respectively (Fig. 8). For thicker scales, the cubic term D increased with oxide-scale thickness. At 800°C, the cubic-term value was close to 100% for a scale thickness of 20 μm. The cubic behavior corresponded to the observed decrease in instantaneous k_p (Fig. 7).

Correlation between Growth Kinetics and Microstructures of NiO Scales

The NiO surface morphology, internal oxide-scale microstructure (described in Part I of this paper) and scale-growth kinetics are compared in an Arrhenius plot (Fig. 9). At high temperatures (>1000°C), and for oxide scales thicker than 5 μm, NiO growth kinetics were parabolic. Internal microstructures of oxide scales were simplex compact characterized by faceted grains. The effect of substrate orientation on oxide grain size and oxide-scale thickness was significant. Microstructures of thinner oxide scales (<5 μm) remained unknown as oxidation time was too short. The study of weight gain corresponding to an oxide-scale thickness ranging from 1 to 5 μm allowed characterization of the significant linear term of kinetic law (Eq. 2). Therefore, the growth of the first 5 μm oxide could strongly depend on some transient step (nucleation) and/or on interfacial reactions. This hypothesis could explain the large effect of nickel orientation on oxide grain size at these temperatures.

The oxidizing temperature of 900°C corresponded to a transient temperature as a change of slope in Arrhenius plot was observed. The growth kinetics of the oxide scale were a mixture of parabolic and cubic laws. The microstructure was simplex (characteristic of highest temperatures), but exhibited numerous pores. Furthermore, the growth of large platelets was observed at the surface of oxide scales. Growth mechanisms of oxide scales were more complex at this temperature than for higher temperatures.

At lower temperatures (<900°C), and for scale thickness of approximately 1 μm, the morphology is cellular and the internal microstructure of oxide scale is simplex porous. Values of k_p are much higher than those predicted from extrapolation from higher temperatures. For thick scales (>5 μm), growth kinetics are a mixture of parabolic and cubic laws. The internal microstructure of oxide scales is duplex and could not be explained by the mechanism of cation bulk diffusion only. Growth of platelets was observed at these temperature and oxide-scale thickness ranges. The effect of substrate orientation on scale microstructures is significant.

DISCUSSION

The set of experimental data (microstructural observations and kinetics study of NiO growth) reported here demonstrates the limits of known kinetics models for the high-temperature oxidation of pure materials. Indeed, the present data confirm that the growth of NiO scales on pure Ni does not obey simple parabolic growth kinetics: (1) the ($\Delta m, t^{1/2}$) weight-gain curves are not linear, showing a deviation to the simple parabolic law ($\Delta m^2 = k_p t$); (2) the observed decrease in k_p with increasing oxide-scale thickness implies

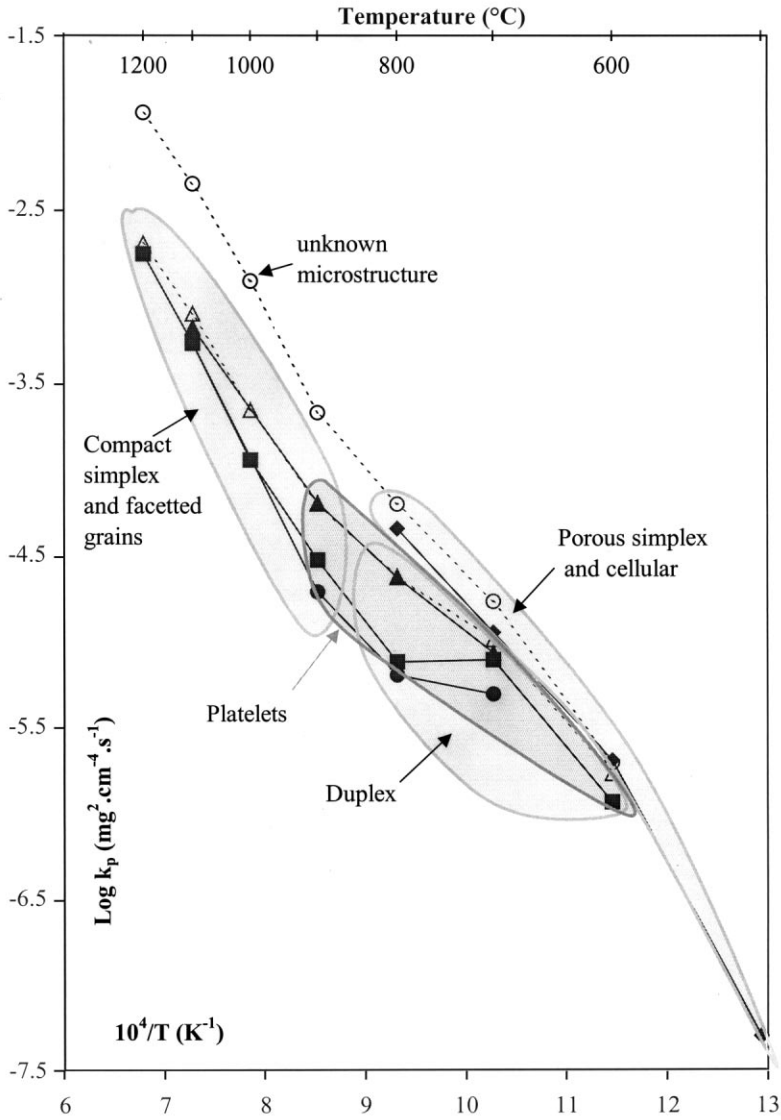

Fig. 9. Arrhenius plot of global parabolic rate constants k_p as a function of test temperature and scale thickness indicating NiO scales morphologies and microstructures.

that the scale-growth kinetics could not be described by the complete formula for parabolic kinetics ($t = a + b\Delta m + c\Delta m^2$) with constant coefficients, and, furthermore, the usual rate equation leading to parabolic growth could not be used; (3) the observed departure from the parabolic kinetics appeared to depend on temperature, scale thickness, and scale microstructure.

The possible effect of grain-boundary diffusion can be inferred from the Arrhenius plot. The three solid lines drawn in Fig. 10 show the parabolic rate constants k_p as a function of temperature, calculated from Atkinson *et al.*[4,24] for the bulk diffusion (Fig. 10, line a) and grain-boundary diffusion of Ni cations for average oxide grain sizes of 10 and 0.5 μm (Fig. 10, lines b and c, respectively). These lines demonstrate that, in the conditions of the present work, the grain-boundary diffusion of Ni cations could still contribute to NiO growth kinetics at temperatures as high as 1200°C. However, the two changes in slope already seen in Fig. 6 (the first one at approximately 900°C and the second one at approximately 700°C) could not be explained only by the effect of grain-boundary diffusion without considering a large and concomitant evolution of scale microstructure, i.e., grain size and grain shape.

In the present work, the oxide grain sizes were roughly estimated from SEM examinations of scale surface or fracture. NiO grain size varies largely with the surface orientation of Ni grains. Figure 11 is representative of the surface morphology and internal microstructure of 10-μm thick oxide scales grown at 1100°C. The main feature of this scale is the clear influence of nickel orientation on scale thickness and oxide grain size so that no average grain size could be accurately determined. Nevertheless, a semiquantitative analysis could be considered, comparing oxide-scale thicknesses and oxide grain size. From comparison of *A* and *B* areas in Fig. 11, it is obvious that the smaller NiO grain size corresponds to a thicker scale. This observation could be explained considering the contribution of nickel grain-boundary diffusion. According to the Atkinson *et al.* data and theory, taking into account bulk and grain-boundary diffusion[4,24] a NiO grain size ratio greater than 3 (as can be seen in Figs. 11a and c) should correspond to an oxide-scale thicknesses ratio greater than 1.5 at this temperature. This calculated difference in oxide-scale thicknesses is illustrated in Fig. 11b with white rectangles. Assuming that the diffusion coefficients were accurately determined, this comparison of NiO-scale thicknesses and oxide grains sizes demonstrates that mechanisms other than bulk and grain-boundary diffusion may influence oxidation kinetics.

The observed change in k_p as a function of scale thickness (Fig. 7) was also used to calculate the variation of oxide grain size from the relation between k_p, bulk diffusivity, grain-boundary diffusivity, and scale grain size, as given by Atkinson.[4,24] This calculation was performed from scale-growth

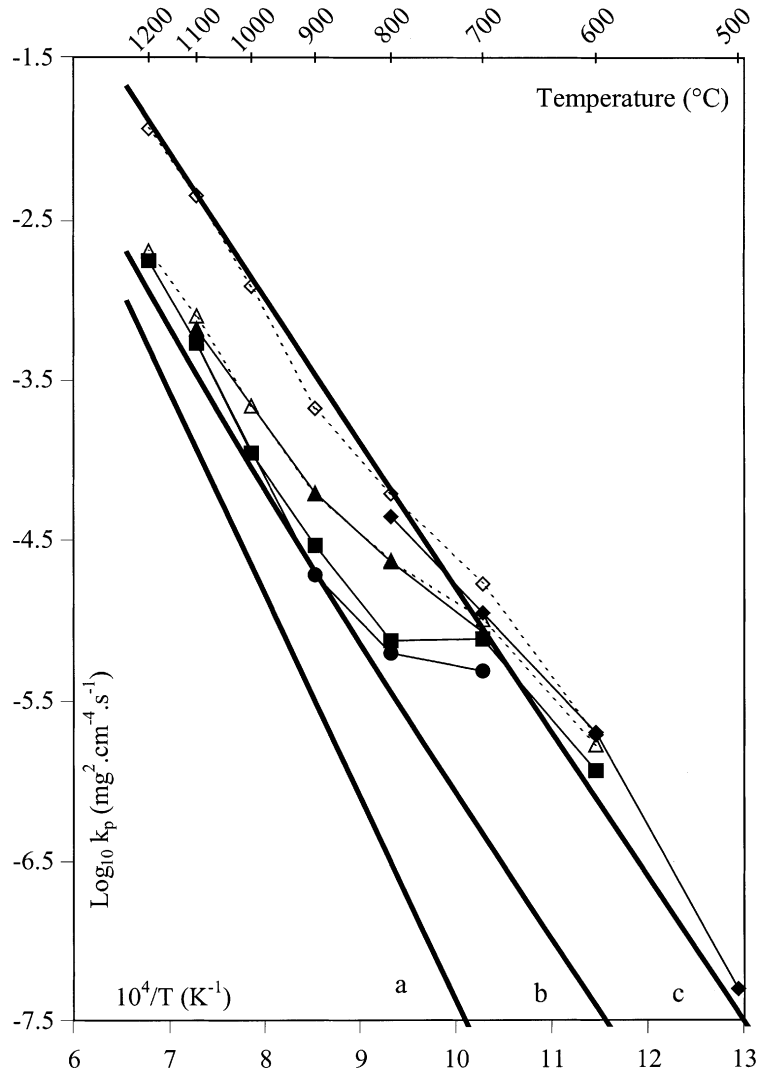

Fig. 10. Arrhenius plot of global parabolic rate constants k_p as a function of test temperature and scale thicknesses of approximately 1 (◆), 5 (▼), 10 (■), and 30 μm (●). White symbols indicated values of k_p calculated for scales thicknesses of 1 (◇) and 5 μm (△) from weight-gain curves of experiments corresponding to oxide-scale thickness of approximately 10 μm. Solid lines were calculated from Atkinson's data [4,24] for bulk (a), and grain-boundary diffusion with NiO with grain size of $g = 10\,\mu$m (b), and $g = 0.5\,\mu$m (c).

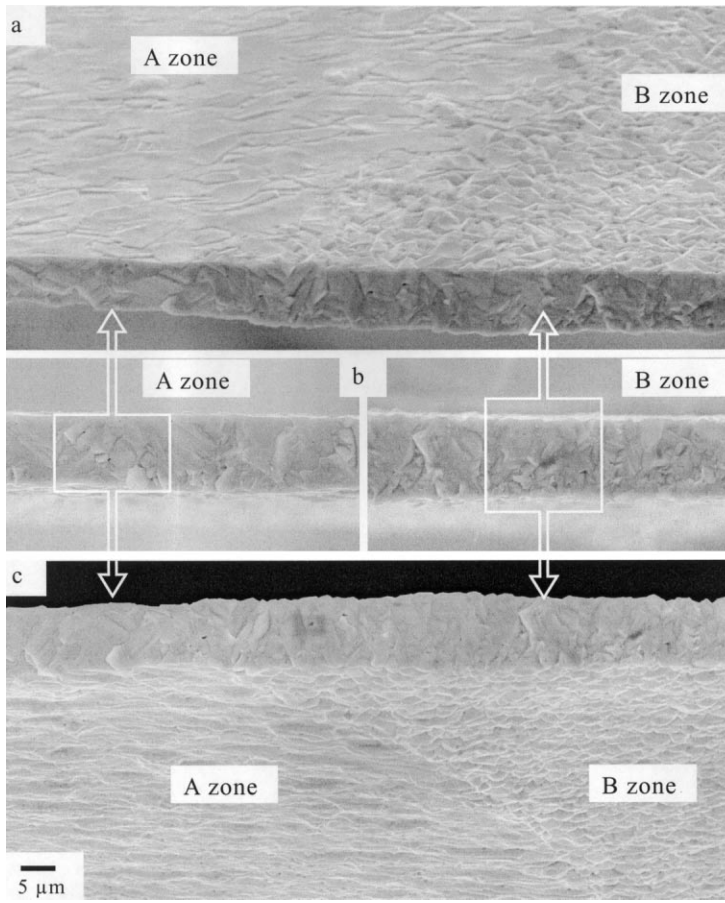

Fig. 11. Effect of substrate orientation on the microstructure of NiO scale 10 μm thick obtained at 1100°C: (a) morphology of the gas–scale interface; (b) fracture; (c) morphology of the scale–metal interface. Areas *A* and *B* correspond to two different NiO microstructures grown on two different crystallographic orientations of nickel.

kinetics at 700, 800, 900, and 1100°C (Fig. 12). The grain size calculated in this way did not present significant evolution during scale growth at 700 and 1100°C for scale thicknesses of 5 up to 30 μm. On the contrary, a large evolution of grain size would be necessary to explain the observed variation of k_p during scale growth at 800 and 900°C. Comparison of these calculated values with surface morphologies of corresponding oxide scales (Fig. 13) clearly showed that the grain-boundary diffusion contribution could not

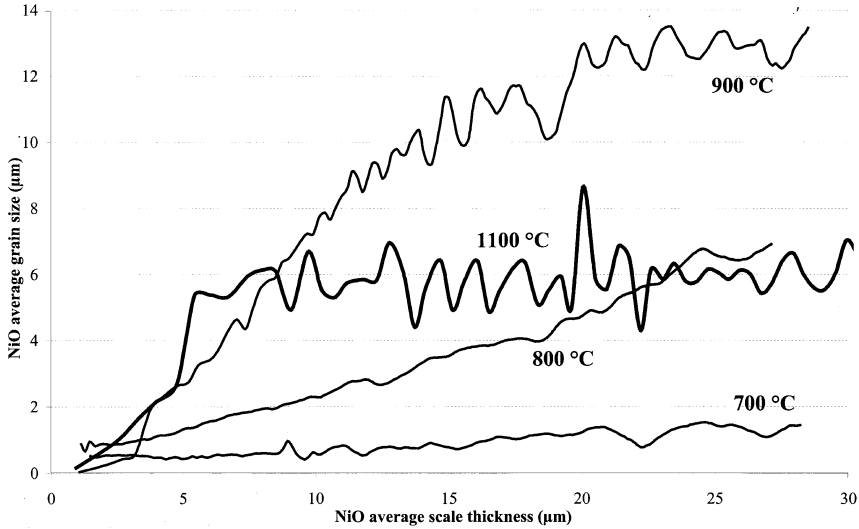

Fig. 12. Variation of oxide grain size calculated from Atkinson *et al.*[4,24] diffusion data in order to fit the observed variation of instantaneous k_p shown in Fig. 6 as a function of scale thickness at 700, 800, 900, and 1100°C.

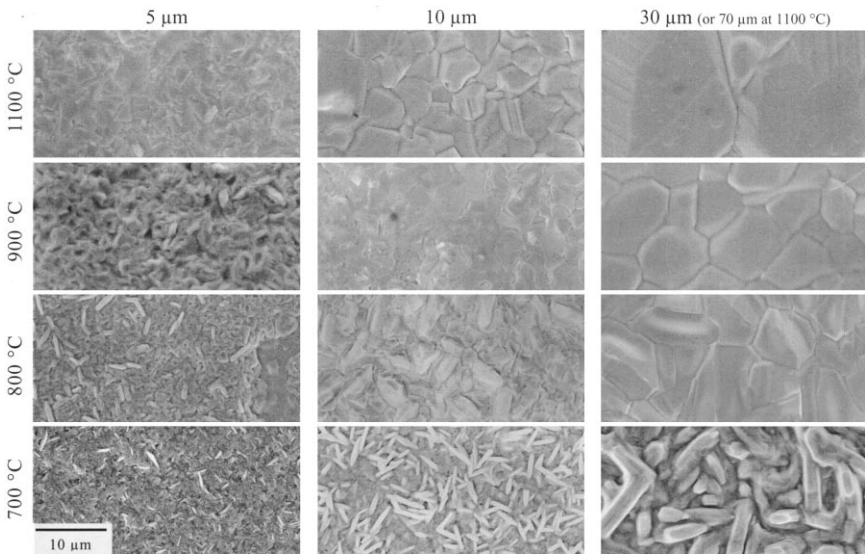

Fig. 13. Surface morphology of NiO oxide scale as a function of temperature and oxide-scale thickness.

be quantitatively demonstrated, even for simplex scales obtained at higher temperatures. For intermediate temperatures (ranging from 600 to 800°C), the large effect of substrate orientation and the very complex microstructure (duplex scale, porosity, channels) makes the direct determination of oxide grain size from micrographs impossible. Moreover, the decrease of k_p with scale thickness and the mixture of cubic and parabolic laws, indicates that any of the known kinetics laws is appropriate to analyze NiO-scale growth in this temperature range.

CONCLUSION

A careful analysis of NiO scale-growth kinetics and NiO scale morphology and microstructure was performed on Ni specimens of high purity and of reproducible microstructure and surface finish. This analysis showed that the oxidation behavior of this quite simple $Ni/NiO/O_2$ system is, in fact, more complex than usually considered. For temperatures higher than 1000°C, the simplex compact layer obeyed a pure parablic kinetic growth for scales thicker than 5 μm. Nevertheless, the substrate-orientation effect on oxide grain size and on oxide-scale thickness could not be explained considering only nickel bulk diffusion. The quantitative demonstration of the grain-boundary diffusion at these temperatures was questioned. For intermediate temperatures (<900°C), the duplex-scale microstructure obeyed complex growth kinetics: decrease in k_p with scale thickness and a mixture of cubic and parabolic laws, indicating that no simple kinetics law is appropriate to analyze NiO-scale growth in this temperature range. More importantly, the model of grain-boundary diffusion cannot be predictive as long as the nickel-oxide microstructure canot be predicted. Therefore, scale-growth kinetics and scale microstructures would be related by a more complicated relationship than usually reported. A better understanding of the NiO growth mechanisms (taking into account duplex-scale growth, platelets growth, and pore formation, etc.) would be required to determine a more realistic, growth-kinetics law. The key to oxidation-kinetics prediction relies on the ability to predict oxide-scale microstructure in relation to substrate crystallographic orientation, chemistry, and surface finish.

REFERENCES

1. M. T. Shim and W. J. Moore, *J. Chem. Phys.* **26**, 802 (1957).
2. R. Lindner and A. Akerstom, *Discussions Faraday Soc.* **23**, 133 (1957).
3. M. L. Volpe and J. Reddy, *J. Chem. Phys.* **53**, 1117 (1970).
4. A. Atkinson and R. I. Taylor, *J. Mater. Sci.* **13**, 427 (1978).
5. A. Atkinson and R. I. Taylor, *Phil. Mag. A*, **39**, 581 (1979),
6. B. Lesage, A. M. Huntz, and P. Lacombe, *Solid State Ionics* **12**, 359 (1984).

7. K. Fueki and J. B. Wagner, Jr., *J. Electrochem. Soc.* **112**, 384 (1965).
8. M. J. Moore and J. K. Lee, *Trans. Faraday Soc.* **48**, 916 (1952).
9. L. Berry and J. Paidassi, *Sci. Rev. Metall.* **65**, 651 (1968).
10. L. Berry and J. Paidassi, *C. R. l'Acad. Sci. Paris C* **262**, 1353 (1966).
11. M. J. Graham, G. I. Sproule, D. Caplan, and M. J. Cohen, *J. Electrochem. Soc.* **119**, 883 (1972).
12. E. A. Gulbransen and K. F. Andrew, *J. Electrochem. Soc.* **101**, 128 (1954).
13. J. C. Pivin, J. Morvan, and D. Mairey, *Acta Metall.* **32**, 2203 (1984).
14. F. Czerwinski and W. W. Smeltzer, *J. Electrochem. Soc.* **140**, 2606 (1993).
15. F. Czerwinski, G. I. Sproule, M. J. Graham, and W. W. Smeltzer, *Corros. Sci.* **37**, 541 (1995).
16. K. R. Lawless, F. W. Young, and A. T. Gwathmey, *J. Chim. Phys.* **53**, 667 (1956).
17. R. Herchl, N. N. Khoi, T. Homma, and W. W. Smeltzer, *Oxid. Met.* **4**, 35 (1972).
18. N. N. Khoi, W. W. Smeltzer, and J. D. Embury, *J. Electrochem. Soc.* **122**, 1495 (1975).
19. M. J. Graham, R. J. Hussey, and M. J. Cohen, *J. Electrochem. Soc.* **120**, 1523 (1973).
20. F. Czerwinski and J. A. Szpunar, *Acta Mater.* **46**, 1403 (1998).
21. L. Berry and J. Paidassi, *Mem. Sci. Rev. Metall.* **LXVII**, 477 (1970).
22. A. Atkinson, R. I. Taylor, and P. D. Goode, *Oxid. Met.* **13**, 519 (1979).
23. A. Atkinson, R. I. Taylor, and A. E. Hugues, *Phil. Mag. A* **45**, 823 (1982).
24. A. Atkinson and R. I. Taylor, *Phil. Mag. A* **43**, 979 (1981).
25. A. A. Moosa, S. J. Rothman, and L. J. Nowicki, *Oxid. Met.* **24**, 151 (1985).
26. E. G. Moya, G. Deyme, and F. Moya, *Scripta Metall.* **24**, 2447 (1990).
27. F. Barbier, J. Bernardini, F. Moya, and M. Déchamps, *Mater. Sci. Res.* **21**, 549 (1987).
28. A. Marrouche, F. Barbier, M. Déchamps, and A. Revcolevschi, *Surface Sci.* **162**, 550 (1985).
29. M. Déchamps, *J. Phys.* **C1**, 309 (1986).
30. A. Atkinson, D. P. Moon, D. W. Smart, and R. I. Taylor, *J. Mater. Sci.* **21**, 1747 (1986).
31. T. Karakasidis and M. Meyer, *Phys. Rev. B* **55**, 13853 (1997).
32. T. E. Karakasidis and G. A. Evangelakis, *Surf. Sci.* **436**, 193 (1999).
33. G. Dhalenne, S. Revcolevski, and C. Monty, *Simkovitch Stubican (Eds), 1985. NATO ASI B* **129**, 371 (1985).
34. D. Monceau, R. Peraldi, and B. Pieraggi, *Defect and Diffusion Forum*, **194**, 1675 (2001).
35. J. Perrow, W. W. Smeltzer, and J. O. Embury, *Acta Metall.* **16**, 1209 (1968).
36. F. N. Rhines and R. G. Connell, Jr., *J. Electrochem. Soc.* **124**, 1122 (1977).
37. F. N. Rhines, R. G. Connell, and M. S. Choi, *J. Electrochem. Soc.* **126**, 1061 (1979).
38. M. J. Graham and M. Cohen, *J. Electrochem. Soc.* **119**, 879 (1972).
39. D. Monceau and B. Pieraggi, *Oxid. Met.* **50**, 477 (1998).
40. D. Caplan, M. J. Graham, and M. Cohen, *J. Electrochem. Soc.* **119**, 1205 (1972).
41. F. A. Elrefaie, A. Manolescu, and W. W. Smeltzer, *J. Electrochem. Soc.* **132**, 2489 (1985).
42. J. J. Gonzalez-Bajanchi, Ph.D. thesis, Institut National Polytechnique de Toulouse, 1995.
43. M. O'Keefe and W. J. Moore, *J. Phys. Chem.* **65**, 1438 (1961).
44. M. Meyer, S. Barbezat, C. El Houch, and R. Talon, *J. Phys.* **41**, 327 (1980).
45. C. Dubois, C. Monty, and J. Philibert, *Phil. Mag. A* **46**, 419 (1982).
46. J. Cabrera-Cano, A. Dominguez-Rodriguez, R. Marquez, J. Castaing, and J. Philibert, *Phil. Mag. A* **46**, 397 (1982).
47. C. Dubois, C. Monty, and J. Philibert, *Solid State Ionics* **12**, 75 (1984).
48. A. Atkinson, F. C. W. Pummery, and C. Monty, in *Transport in Nonstoichiometric Compounds*, G. Simkovitch and V. S. Stubican (eds). (Plenum, New York, 1985), pp. 359–370.
49. A. Atkinson and R. I. Taylor, *Phil. Mag. A* **43**, 979 (1981).